Refinement of the pressure-temperature phase diagram of the organic superconductor with asymmetric anions $(TMTSF)_2FSO_3$

Y. J. Jo, E. S. Choi, Haeyong Kang, and W. Kang*
Department of Physics, Ewha Womans University, Seoul 120-750, South Korea

I. S. Seo and O. H. Chung
Department of Physics, Sunchon University, Sunchon 540-742, South Korea

(Received 28 June 2002; revised manuscript received 19 August 2002; published 17 January 2003)

The pressure-temperature phase diagram of the organic superconductor $(TMTSF)_2FSO_3$ is refined by performing measurements of the interlayer resistance (R_{zz}) and the longitudinal thermoelectric power (S_{xx}). In addition to refining the phase transitions previously discussed in the literature, the results show at least two new phase changes at high pressure. The complexity of the phase diagram suggests that the finite electric dipole moment of the asymmetric FSO_3 anions, which gives these anions an additional degree of freedom, should be taken into account in addition to their structural ordering.

DOI: 10.1103/PhysRevB.67.014516 PACS number(s): 74.70.Kn, 74.25.Fy, 71.30.+h

I. INTRODUCTION

Bechgaard salts $(TMTSF)_2X$ ($X=PF_6$, AsF_6, ClO_4, ReO_4, etc.) undergo numerous interesting phase transitions related to competition among various ground states, such as superconducting (SC), metallic, insulating spin-density-wave (SDW), and charge-density-wave (CDW) states. External hydrostatic pressure plays a major role in these phase transitions because changes in the pressure induce anisotropic changes in the electron transfer integral between TMTSF molecules. The characteristics of the phase transitions in Bechgaard salts and their critical temperatures also depend on the size and symmetry of the anions, because increasing the anion size works as a negative internal pressure and the ordering of asymmetric anions creates superlattice potentials with various periodicities.[1]

The Bechgaard salts with centrosymmetric anions such as $X=PF_6$, AsF_6, SbF_6 undergo a metal-to-insulator (MI) transition to the SDW state at around 12 K during cooling.[2,3] However, the SDW transition is suppressed at pressures higher than about 6 kbar, and the SC state appears at temperatures below $T_c=1.2$ K.[4] In salts with noncentrosymmetric anions such as ClO_4, ReO_4, and NO_3, on the other hand, the anions usually undergo orientational ordering and form a superlattice potential with a range of periodicities. When the ClO_4 salt is slowly cooled at ambient pressure, the anion ordering (AO) with wave vector $\mathbf{q}_1=(0,1/2,0)$ occurs below 24 K (Ref. 5) and the SC state stabilizes below 1.4 K.[6] Thermal quenching of the same system leads to the insulating SDW ground state with disordered anions below 6 K.[7] In the ReO_4 salt, the AO with $\mathbf{q}_2=(1/2,1/2,1/2)$ (Ref. 8) leads to an insulating state below 180 K at ambient pressure.[9] Under pressures higher than about 8 kbar, another type of AO with $\mathbf{q}_3=(0,1/2,1/2)$ dominates[10] and the SC state emerges below 1.3 K.[11] In the NO_3 salt, the planar NO_3 anions order with $\mathbf{q}_4=(1/2,0,0)$ at around 45 K (Ref. 12); the metallic nature of this salt remains intact through this transition, and on further cooling a transition to a SDW state starts at around 10 K.[13] The metallic state is recovered above 8 kbar without any sign of superconductivity for pressures up to 24 kbar and temperatures down to 50 mK.[14]

Additional effects due to permanent electric dipole moments residing on the anions have been studied for the salt $(TMTSF)_2FSO_3$.[15–17] The tetrahedral structure of the FSO_3 anion, in which the S atom lies at the center, resembles the structures of other tetrahedral anions such as ClO_4 and ReO_4. However, the asymmetric distribution of two types of atoms with different electronegativities at the four apices in FSO_3 causes this anion to have a permanent electric dipole moment. At ambient pressure, $(TMTSF)_2FSO_3$ undergoes a MI transition at around 89 K with formation of the anion superstructure with $\mathbf{q}_2=(1/2,1/2,1/2)$.[18] However, the structural ordering of the FSO_3 anions can only be considered complete when their electric dipole moments are ordered. No information is currently available on the ordering of dipole moments in $(TMTSF)_2FSO_3$.

According to the first pressure-temperature (P-T) phase diagram of $(TMTSF)_2FSO_3$ to be reported, the MI transition temperature decreases almost linearly with increasing pressure up to 6 kbar.[16] In the region between 5 and 6 kbar, the temperature dependence of the resistance depended on the cooling rate. A superconducting transition with T_c greater than 3 K, the highest in the TMTSF family, was reported for pressures greater than 5 kbar. Subsequently, Tomić determined a more detailed phase diagram of $(TMTSF)_2FSO_3$.[19] In this phase diagram, the MI transition temperature increased slowly to 94 K at 13 kbar, where the transition temperature at each pressure was identified as a change in the slope of a plot of resistance versus temperature. In addition, another transition line similar to that in the first phase diagram was also reported over broader range from 3 to 7.5 kbar below which the resistance depended on cooling rates. The relative simplicity of the two previously reported P-T phase diagrams for $(TMTSF)_2FSO_3$ is somewhat surprising, given that FSO_3 anions have an additional degree of freedom associated with the electric dipole moment.

In the time since the phase diagrams described above were determined, a more reliable pressure generating system

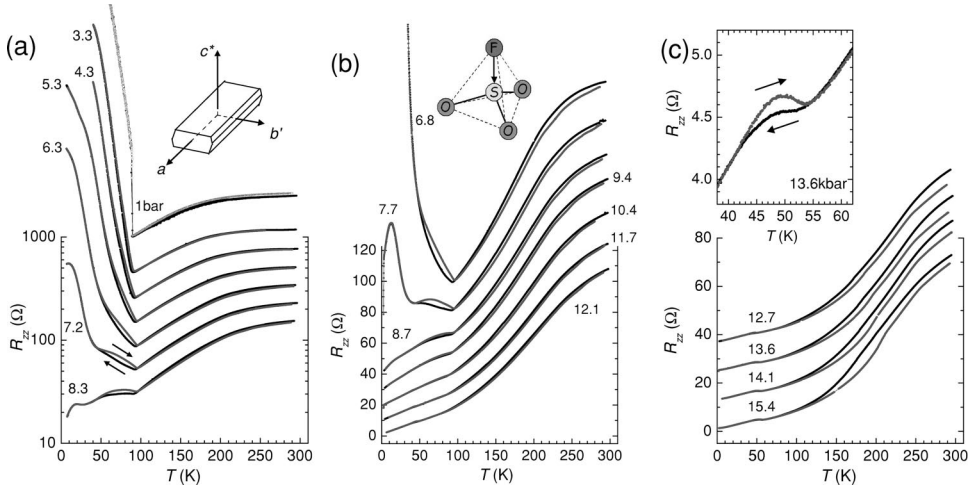

FIG. 1. Temperature dependence of interlayer resistance at pressures of from 1 bar to 15.4 kbar. Each set of data was obtained with a separate sample. (a) Low-pressure data; plotted on a logarithmic scale. (b) and (c) Intermediate- and high-pressure data, plotted on a linear scale. The base lines of successive curves are shifted equally for clarity. The hysteresis observed at around 50 K at high pressure is enlarged in the inset of (c). The pressures cited in this figure are the room-temperature values.

has been developed for which the temperature characteristics of the pressure medium are better understood. So we carried out a new investigation of the phase diagram of $(TMTSF)_2FSO_3$ through electric resistance and thermoelectric power measurements. The two measurements provided complementary data that could be used to identify and cross-check the phase behavior. Our results reveal at least two new phase transitions and refine the previously reported phase transitions.

II. EXPERIMENTS

$(TMTSF)_2FSO_3$ crystals were grown by electrocrystallization from commercially available TMTSF molecules and home-prepared tetrabuthylammonium-FSO_3. To measure the interlayer resistance (R_{zz}), two 20 μm annealed gold wires were attached onto each (001) surface of the samples with silver paste and the standard four-probe technique with a lock-in amplifier was adopted.

A novel technique was developed to measure the thermoelectric power under pressure. The thermocouples and electric lead wires were directly glued to the sample ends with Stycast 2850 epoxy to enhance the thermal integration and to avoid any undesirable pressure medium effects. The temperature difference (ΔT) was maintained at less than 0.1 K over the entire temperature range. Even after careful arrangement of the sample, the pressure medium still had an effect on the thermoelectric power, which manifested as a very small change near the solidification point of the pressure medium. However, the effect was so small compared to the thermoelectric power signal of the sample that we considered thermal integration to be sufficiently accurate for this work. The effect of pressure on the thermocouples is ignored in the data presented here (see below). We also ignore the effect of pressure on the gold electrical lead wires used in this work because it is believed to be very small.[20] The validity of this assumption was supported by the observation of a pressure-independent thermoelectric power of the $YBa_2Cu_3O_{7-x}$ superconductor below the transition temperature. In the high-temperature range, the effect would be even smaller because the thermoelectric power of the samples becomes large. Indeed, previous thermoelectric power measurements of gold wires showed that the thermoelectric power at room temperature decreases by about 0.07 μV/K on increasing the pressure from 1 bar to 15 kbar.[20] The details of the thermoelectric power measurements under pressure are published separately.[21]

Pressures of up to 16 kbar were generated in a BeCu clamp cell with a 1:1 mixture of Daphne 7373 oil and kerosene oil as the pressure medium. This mixture was chosen because it has several advantageous characteristics: (1) pressure does not change discontinuously through its solidification, (2) pressure decreases approximately linearly with decreasing temperature and is independent of the initial pressure at room temperature,[22] and (3) solidification and melting of the oil are so mild that the same sample can be recycled for systematic pressure studies, which greatly facilitates the comparison between curves at adjacent pressures. Because the pressure decreases continuously with decreasing temperature, the pressure at room temperature is used to describe the $R_{zz}(T)$ and $S_{xx}(T)$ curves throughout this paper. However, the corrected pressure at each temperature is used for presenting the superconducting transition and the phase diagram.

III. RESULTS AND DISCUSSION

A. Resistance measurements

Figure 1 shows the temperature dependence of R_{zz} measured over three overlapping pressure ranges, where a different sample was used for each pressure range. The curve at ambient pressure was obtained separately. First, we will focus on the data below 8.3 kbar. The MI transition previously reported to be at around 90 K is clearly observed at 89 K at the ambient pressure. (We will call it transition I.) The sudden jump in the resistance by an order of magnitude at the transition is characteristic of a first-order transition. R_{zz} is activated on further cooling with a gap (Δ/k_B) of $\sim$770 K. Interestingly, this first-order behavior disappears as soon as the pressure is applied, but the transition is still evident at least up to 10.4 kbar either as a sharp upturn in the resistance or as a change in the slope of the resistance curve. Although R_{zz} increases rapidly below transition I for pressures of less

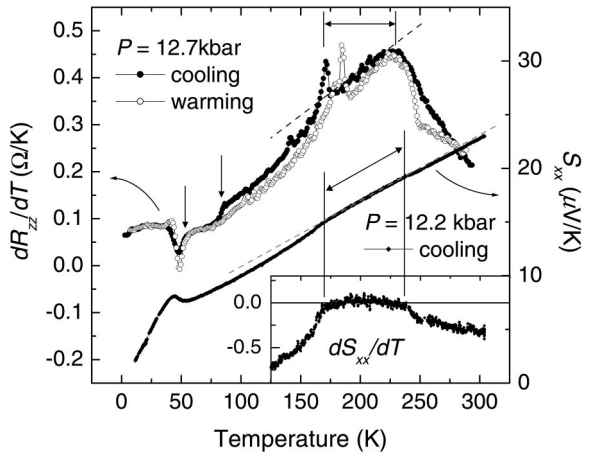

FIG. 2. dR_{zz}/dT at 12.7 kbar and S_{xx} at 12.2 kbar. The maximum of dR_{zz}/dT corresponds to solidification of the pressure medium. A sharp peak in dR_{zz}/dT separates the region where dR_{zz}/dT is almost linear from the region where it is a faster function of temperature. $S_{xx}(T)$ is linear in the same temperature interval. Other transitions are also evident in dR_{zz}/dT, as indicated with downward arrows. $dS_{xx}(T)/dT$ in the inset shows the good linearity of $S_{xx}(T)$ between 170 K and 235 K.

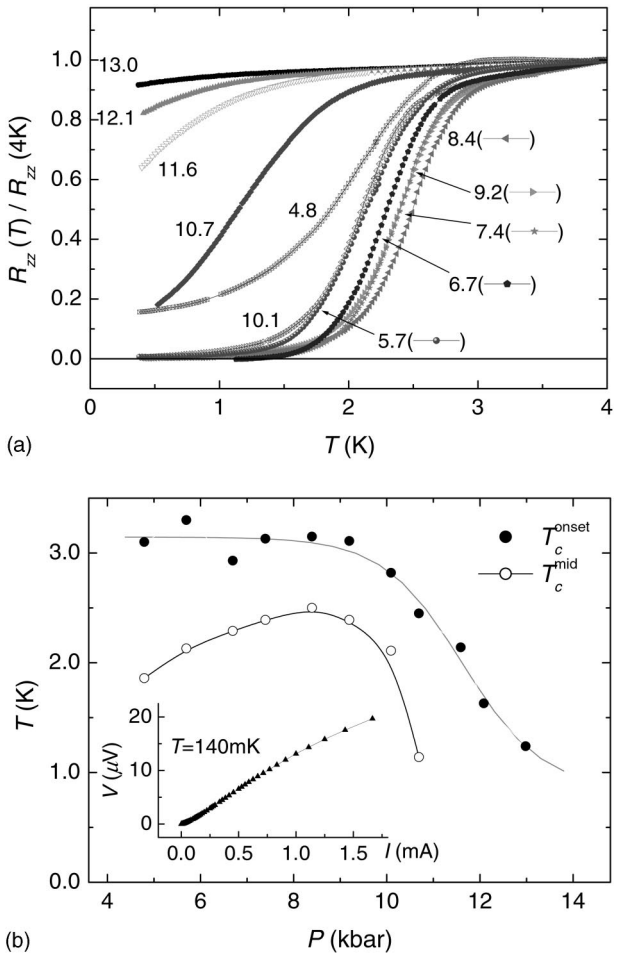

FIG. 3. (a) Superconducting transitions of $(TMTSF)_2FSO_3$ at various pressures. Each resistance curve is normalized by the resistance at 4.0 K. The general tendency of the superconducting transition is continuous although the resistance at 4 K varies more than three orders of magnitude between 4.8 and 13.0 kbar. (b) Pressure dependence of the superconducting transition temperature. Both T_c^{onset} and T_c^{mid} are shown. Lines are guides to the eyes only. The inset shows *I-V* characteristics at 140 mK under $P=8.8$ kbar.

than 7 kbar, it is not activated and tends to saturate as the temperature is lowered. This behavior stands in contrast to that of $(TMTSF)_2ReO_4$, which suffers the same (1/2, 1/2, 1/2) anion ordering transition but for which the resistance jump at the MI transition is conserved and the resistance shows activated behavior until at least 7.7 kbar.[23] This observation implies that the transition I in $(TMTSF)_2FSO_3$ does not open a gap over the entire Fermi surface, even at very low pressure.

One of the new features revealed in the present study is that the MI transition at 89 K splits into two transitions under pressure, as is clearly shown in Fig. 1(a). Although the second transition (denoted transition II) is much less evident at low pressures, it can be unambiguously identified either from the discontinuity in the slope of the resistance curve and/or from the disappearance of hysteresis. The temperatures at which transitions I and II take place seem to converge at ambient pressure (see the phase diagram presented in Fig. 6). As the pressure is increased, transition II takes place at progressively lower temperatures whereas the temperature of transition I remains more or less constant.

The region between the two transitions is characterized by strong hysteresis. $R_{zz}(T)$ is always larger during warming than during cooling under the same conditions (see arrows on the 7.2 kbar curves in Fig. 1). Although transition II smears out above 8.7 kbar, the hysteresis clearly persists up to 9.4 kbar [Fig. 1(b)]. Below transition II, the resistance rapidly increases at low pressures but tends to saturate as the temperature is lowered further, and even decreases on further cooling for pressures between 7.2 and 8.3 kbar. Tomić attributed the hysteresis between transitions I and II to incomplete development of order parameter.[19] However, the clearly discontinuous nature of transition II and its reproducibility rule out this possibility. Taking a closer look at the intermediate-pressure data (e.g., 7.7 kbar), neither transition I nor transition II looks like a MI transition for which an energy gap is formed over the entire Fermi surface. Instead, the two transitions are strongly reminiscent of the behavior of $NbSe_3$, in which two successive CDW transitions open a gap over only a part of the Fermi surface and the resistance shows jumps at each transition before recovering metallic behavior at lower temperature.[24] This point will be discussed in greater detail in relation to the thermoelectric power data presented in Sec. III B.

It is well known that (1/2, 1/2, 1/2) anion ordering induces a MI transition for TMTSF salts such as $(TMTSF)_2ReO_4$ and $(TMTSF)_2BF_4$,[18] and that increasing the hydrostatic pressure simultaneously reduces the MI transition temperature and the energy gap. It is very unusual to have two successive transitions and reentrance to the metallic state after the system has undergone (1/2, 1/2, 1/2) ordering. The previous low-temperature x-ray study of $(TMTSF)_2FSO_3$ was carried out only at 87 K and at ambient pressure. Until a detailed x-ray analysis is carried out under pressure and at

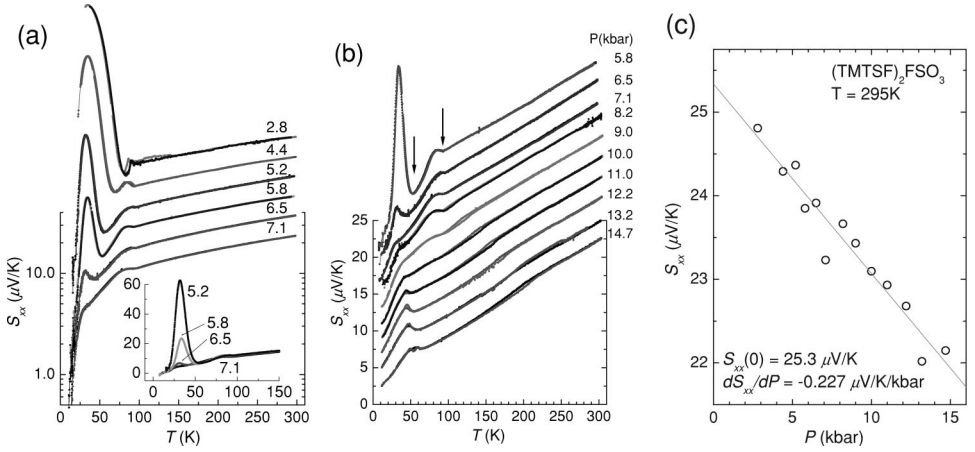

FIG. 4. Temperature dependence of thermoelectric power of $(TMTSF)_2FSO_3$ at various pressures. To facilitate the comparison, low-pressure data are plotted on a logarithmic scale (a) and high-pressure data on a linear scale (b). The base lines of successive curves are shifted equally for clarity. Inset of (a) reproduces the data at 5.2, 5.8, 6.5, and 7.1 kbar on the linear scale. The pressure dependence of the thermoelectric power at 295 K is depicted in (c).

lower temperatures, we can only speculate that the additional features observed in the present study are related to the nonzero electric dipole moments of the FSO_3 anions (a kind of ferroelectric or antiferroelectric transition).

Another new feature of the $(TMTSF)_2FSO_3$ phase diagram uncovered in the present study is a bumplike transition (transition III) at around 50 K for pressures above 10 kbar. This transition is accompanied by a well-defined small hysteresis, which grows with increasing pressure. A representative example of the behavior of R_{zz} at transition III is shown in the inset of Fig. 1(c). The resistance is again larger in the warming curves than in the cooling curves. The transition temperature increases slowly as the pressure is increased. The pressure and temperature characteristics of transition II at low pressure and of transition III at high pressure are very similar to those of the (1/2, 1/2, 1/2) and (0, 1/2, 1/2) anion ordering transitions of $(TMTSF)_2ReO_4$.[10] However, we cannot proceed further without direct evidence such as that provided by x-ray diffraction measurements.

The first derivative of R_{zz}, dR_{zz}/dT, undergoes an abrupt change with increasing temperature. Figure 2 shows the temperature dependence of dR_{zz}/dT at 12.7 kbar together with the thermoelectric power at 12.2 kbar for comparison. As the system is cooled from ambient temperature, dR_{zz}/dT has a maximum at a temperature corresponding to the solidification of the pressure medium. The solidification temperature can be unambiguously determined from the thermoelectric power measurements, as mentioned in Sec. III B. dR_{zz}/dT shows a more or less linear temperature dependence (i.e., R_{zz} is quadratic with respect to temperature) over an interval of about 70 K below solidification (shown in Fig. 2). The same temperature interval is also characterized by linear thermoelectric power (see lower curves in Fig. 2 and the discussion below). The thermoelectric power has a large hysteresis just below this temperature region. Although no transition is known to occur at this temperature, we speculate that the observed hysteresis may result from a weak ordering of either anion structure or electric dipole moments because the characteristics of $R_{zz}(T)$ and $S_{xx}(T)$ around the transition temperature are similar to those around the (0, 1/2, 0) anion ordering transition temperature in $(TMTSF)_2ClO_4$.[25]

Figure 3(a) shows the superconducting transitions of $(TMTSF)_2FSO_3$ under various pressures. Pressure values are corrected for the effect of temperature on pressure. In this figure, resistance was normalized with R_{zz}(4 K) to fit all data on the same plot; R_{zz}(4 K) varies from 1.4 to 1350 Ω over the pressure range of 5.7–13.0 kbar. There are two remarkable features in this figure. First, the onset temperature of superconductivity, T_c^{onset}, is exceptionally high compared to the previously reported value.[16] Second, the transition is very broad and incomplete. T_c^{mid} is defined as the temperature at which the resistance drops to 50% of its normal-state value. As depicted in Fig. 3(b), T_c^{onset} is approximately constant from 4.8 kbar to about 9 kbar and then falls very rapidly, whereas T_c^{mid} has a maximum at around 8.5 kbar. T_c^{mid} decreases much faster toward higher pressures than toward lower pressures, and T_c^{mid} cannot be defined above 11.6 kbar. For all of the pressures considered, the superconducting transition is incomplete; a finite resistance remains even far below the superconducting transition temperature, as shown in the inset of Fig. 3(b). This agrees with the suggestion that $(TMTSF)_2FSO_3$ is a filamentary superconductor[17] and with the observation of a very small (less than 2%) Meissner effect in this material.[26]

B. Thermoelectric power measurements

The thermoelectric power along the *a* axis (S_{xx}) under pressures of 2.8–14.7 kbar on two samples (below 7.1 kbar and above) is presented in Figs. 4(a) and 4(b). For comparison, we first summarize the results of previous thermoelectric power measurements by Lacoe *et al.*:[16] (1) room-temperature thermoelectric power increased from 22 to 28 μV/K as pressure was increased from 1 bar to 10 kbar, and (2) thermoelectric power decreased monotonically with decreasing temperature. However, our results differ substantially from those of Lacoe *et al.*[16] First, we found that the thermoelectric power at room temperature decreases more or less linearly with increasing pressure at a rate of -0.23 μV/K per kbar [Fig. 4(c)], with an estimated ambient pressure value of 25.3 μV/K. The overall pressure effect on the Chromel-AuFe 0.07% thermocouples used in the present work was less than 4%, and this effect alone could give a pressure derivative of $dS/dP = -0.06$ μV/K per kbar. We also used Chromel-Constantan thermocouples to measure the thermoelectric power of other TMTSF salts, which gave a

different sign of the pressure derivatives, but we also observed a decrease in S_{xx} with increasing pressure at room temperature. Second, the many interesting phase transitions observed in the resistance measurements are also evident in the behavior of the thermoelectric power.

As shown in Figs. 4(a) and 4(b), transitions I and II clearly appear in the thermoelectric power data as abrupt increases in S_{xx}. Transition II is very clear in S_{xx}, even at low pressures where this transition is indistinct in the R_{zz} data. Transitions I and II at 5.8 kbar are indicated with downward arrows in Fig. 4(b). Interestingly, the thermoelectric power remains within the same order of magnitude even after the two successive transitions and falls again at temperatures below about 30 K. This falloff at low temperature is contrary to the behavior of R_{zz}, which continues to increase in this temperature regime. The thermoelectric power does not show the temperature dependence characteristic of semiconductors ($\propto 1/T$) at any of the imposed pressures. Even at the moderate pressure of 5.2 kbar, the thermoelectric power data indicate that the electron system remains metallic at low temperature, although the resistance is strongly elevated. The reentrance to metallic behavior at low temperature becomes increasingly evident as the pressure increases [inset of Fig. 4(a)]. At 7.1 kbar, the thermoelectric power no longer shows the significant rise observed at lower pressures; instead, only kinks are observed at the transitions. The transition temperatures obtained from the thermoelectric power data follow closely those obtained from the R_{zz} data. The temperature dependence of S_{xx} below 8 kbar as well as that of R_{zz} supports the suggestion that a gap opens over only part of the Fermi surface. Thus, the low temperature ground state is essentially metallic although a substantial portion of the Fermi surface is removed through two transitions. Increasing the pressure gradually reduces the gapped portion of the Fermi surface.

Although the thermoelectric power shows a maximum at around 30 K for pressures below 7.1 kbar, the resistance shows only either a slope change or a small anomaly at this temperature, depending on the sample. For pressures of 5.2 kbar and above, the thermoelectric power converges to zero with decreasing temperature [Fig. 4(a), inset]. According to Ref. 27, 30 K corresponds to the temperature below which a strong electric field can switch the insulating state to a metallic state whose resistance is smaller by a factor of 10^6 at 4.2 K. It was suggested that the application of a strong electric field caused the FSO_3 dipoles to take on ferroelectric order and that the improved uniformity of the crystal potential facilitated electron conduction. In this context, the decrease in the thermoelectric power that we observed below about 30 K can be interpreted as a decrease in the system entropy following the loss of an orientational degree of freedom. Another possible explanation is that two conduction bands with different types of carriers form across transitions I and II. Under this hypothesis, the thermoelectric power maximum would originate from the disappearance of the conductivity contribution from a certain portion of the Fermi surface,[28] and the resistance maximum below 35 K between 7 and 8.5 kbar would reflect the completion of gap opening.

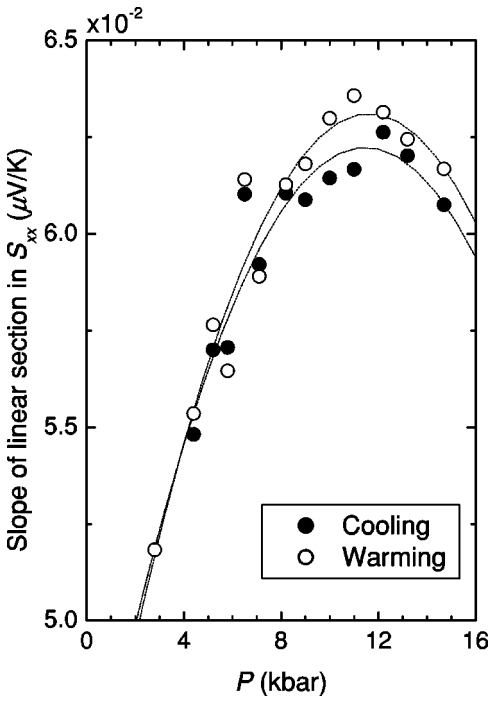

FIG. 5. Pressure dependence of the slope of the linear section of the thermoelectric power.

Between 7.1 and 9.0 kbar, the thermoelectric power shows only a simple kink in the slope at temperatures corresponding to transition II. However, on further increase of the pressure a new transition develops at around the same temperature. The high-pressure bumplike transition is distinguished from the low-pressure transition by the appearance of hysteresis, both in the magnitude of the thermoelectric power and in the transition temperature. It is interesting to note that the transition begins to separate at 14.7 kbar, which is not the case in the resistance. The slope of the thermoelectric power is much steeper below this bump transition than above, which may signify a reduction of the bandwidth across the transition following the simplest one-dimensional tight-binding band model.

The beginning of the solidification of the pressure medium can be detected very precisely by monitoring the temperature difference (ΔT) between two heater blocks driven by alternating currents with the same amplitude but whose phases differ by 90°.[21] Because the amount of heat loss by the pressure medium changes discontinuously through the liquid-solid transition, a small increase of ΔT is clearly observed when the oil begins to solidify. As already mentioned in the discussion of Fig. 2, once the solidification is completed, the thermoelectric power shows a linear dependence on temperature, as is observed for most Bechgaard salts at ambient pressure.[25] The slope at 2.8 kbar is about 5.2×10^{-2} μV/K^2, which is slightly smaller than the value of 7.0×10^{-2} μV/K^2 reported for $(TMTSF)_2PF_6$ at ambient pressure.[25] The slope of the section in which the thermoelectric power depends linearly on temperature, increases with pressure, and has a maximum at around 11 kbar, as shown in Fig. 5. The largest slope is about 6.3×10^{-2} μV/K^2. This

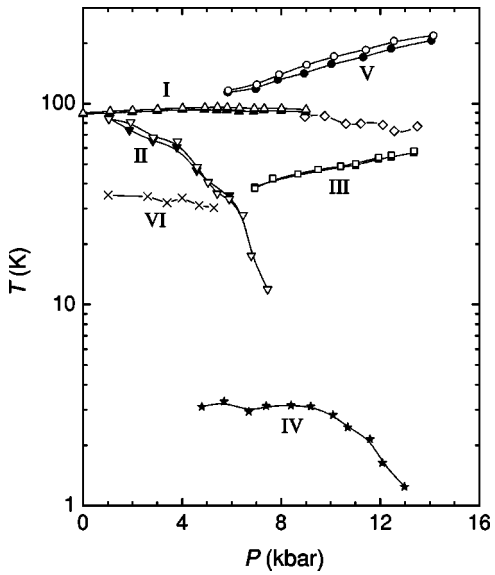

FIG. 6. Pressure-temperature phase diagram of $(TMTSF)_2FSO_3$. The upward triangles (△, ▲) represent the first MI transition (transition I), the downward triangles (▽, ▼) the second MI transition (transition II), the squares (□, ■) the high pressure bump transition (transition III), and the circles (○, ●) the limit of linear (S_{xx}) or quadratic (R_{zz}) temperature dependence. Solid symbols are for cooling and the open ones for warming. The stars (⋆) stand for the superconducting transition. Crosses (×) indicate the temperature where the thermoelectric power has a maximum.

result suggests either that the bandwidth is not a simple decreasing function of pressure for $(TMTSF)_2FSO_3$ or that the one-dimensional tight-binding band model breaks down at high pressure. It is also worth mentioning that the frequency of Shubnikov–de Haas oscillations shows discrete behavior around the pressure at which the temperature coefficient of the thermoelectric power shows a maximum.[29]

C. Phase diagram

Figure 6 shows the phase diagram obtained from the resistivity and thermoelectric power measurements. The effect of the temperature on the pressure is corrected in the phase diagram. The absolute error of the pressure reading is less than 0.2 kbar, and the relative error compared to neighboring points is much less. The reliability of the data is highlighted by the fact that we found excellent agreement between the results obtained using two independent experimental probes over several independent runs with many different samples. The phase diagram of $(TMTSF)_2FSO_3$ can be summarized as follows.

(1) The 89 K transition at ambient pressure splits into two transitions as pressure is applied. The temperature of the first transition (I) is relatively independent of pressure, whereas the temperature of the second transition (II) decreases at a rate of about -10 K/kbar. Transition I becomes difficult to discern above 9 kbar, although a possible remnant of this transition persists until 14 kbar. Transition II disappears completely above 8 kbar.

(2) At pressures greater than 7 kbar, a new phase transition (III) appears at around 35 K. Evidence of this transition is observed in the behavior of both the resistivity and the thermoelectric power. This bumplike transition with hysteresis strengthens with increasing pressure and the transition temperature increases at a rate of about 3.1 K/kbar.

(3) A superconducting transition (IV) occurs at around 3 K at pressures as low as 4.8 kbar. Both T_c^{onset} and T_c^{mid} are the highest in the TMTSF family. However, the superconductivity exhibits features characteristic of a filamentary superconductor.

(4) Above 9 kbar, there is a new transition (V) accompanied by hysteresis. The transition temperature increases and the hysteresis grows with pressure. Above this transition, dR_{zz}/dT and S_{xx} vary linearly with temperature.

(5) The maximum in the thermoelectric power observed at around 30 K (VI) does not reflect an anomaly in the resistance. Below this temperature, the electric dipole moment has previously been reported to exhibit switching behavior under a strong electric field. The source of the maximum in the thermoelectric power remains an open question, because the formation of two conducting bands with different types of carriers may give the same result if a gap opens on one of them.

IV. CONCLUSION

We have revealed that the organic superconductor $(TMTSF)_2FSO_3$, whose anions carry nonvanishing electric dipole moments, has a very rich phase diagram. The previously reported MI transition at around 89 K at ambient pressure splits into two transitions as pressure increases. According to the thermoelectric power data, the ground state may not be an insulating state even at low pressures. The superconducting transition occurs above 4.8 kbar with the highest T_c among Bechgaard salts, but the SC state is marginal. Of particular interest is the discovery of a new cascade of transitions that develops at pressures above 8 kbar, where the low-pressure transitions have mostly disappeared. The appearance of these transitions suggests that a different kind of anion ordering may be induced at high pressure. A detailed x-ray study of each phase is necessary to distinguish the contribution of electric dipole moments from the effect of structural transitions due to anion ordering and to clarify the pressure-induced anion ordering.

ACKNOWLEDGMENTS

This work was supported by the Korea Science and Engineering Foundation under Grant No. R01-2000-000-00036-0 and by the Ministry of Education, Korea under BK21 program.

*Author to whom correspondence should be addressed. Electronic address: wkang@ewha.ac.kr

[1] K. Ishiguro, K. Yamaji, and G. Saito, *Organic Superconductors*, 2nd ed., Vol. 88 of *Series in Solid State Science* (Springer-Verlag, Berlin, 1988).
[2] J. C. Scott, H. J. Pedersen, and K. Bechgaard, Phys. Rev. Lett. **45**, 2125 (1980).
[3] K. Mortensen, Y. Tomkiewicz, T. D. Schultz, and E. M. Engler, Phys. Rev. Lett. **46**, 1234 (1981).
[4] D. Jérome, A. Mazaud, M. Ribault, and K. Bechgaard, J. Phys. (France) Lett. **41**, L (1980).
[5] J. P. Pouget, G. Shirane, K. Bechgaard, and J. M. Fabre, Phys. Rev. B **27**, 5203 (1983).
[6] K. Bechgaard, K. Carneiro, M. Olsen, F. Rasmussen, and C. S. Jacobsen, Phys. Rev. Lett. **46**, 852 (1981).
[7] T. Takahashi, D. Jérome, and K. Bechgaard, J. Phys. (France) Lett. **43**, L565 (1982).
[8] R. Moret, J. P. Pouget, R. Comes, and K. Bechgaard, Phys. Rev. Lett. **49**, 1008 (1982).
[9] C. S. Jacobsen, H. J. Pedersen, K. Mortensen, G. Rindorf, N. Thorup, J. B. Torrance, and K. Bechgaard, J. Phys. C **15**, 2651 (1982).
[10] R. Moret, S. Ravy, J. P. Pouget, R. Comes, and K. Bechaard, Phys. Rev. Lett. **57**, 1915 (1986).
[11] S. S. P. Parkin, D. Jérome, and K. Bechgaard, Mol. Cryst. Liq. Cryst. **79**, 213 (1981).
[12] J. P. Pouget, R. Moret, R. Comes, and K. Bechgaard, J. Phys. (France) Lett. **42**, L5203 (1981).
[13] P. Baillargeon, C. Bourbonais, S. Tomić, P. Vaca, and C. Coulon, Synth. Met. **27**, B83 (1989).
[14] A. Mazaud, Ph.D. thesis, Université Paris-Sud, 1981.
[15] F. Wudl *et al.*, J. Chem. Phys. **76**, 5497 (1982).
[16] R. C. Lacoe, S. A. Wolf, P. M. Chaikin, F. Wudl, and E. Aharon-Shalom, Phys. Rev. B **27**, 1947 (1983).
[17] R. C. Lacoe, P. M. Chaikin, F. Wudl, and E. Aharon-Shalom, J. Phys. (Paris), Colloq. **44**, C3-767 (1983).
[18] R. Moret, J. P. Pouget, R. Comes, and K. Bechgaard, J. Phys. (Paris), Colloq. **44**, C3-957 (1983).
[19] S. Tomić, Ph.D. thesis, Université Paris-Sud, 1986.
[20] F. J. Blatt, P. A. Schroeder, C. L. Foiles, and D. Greig, *Thermoelectric Power of Metals* (Plenum, New York, 1976).
[21] E. S. Choi, H. Kang, Y. J. Jo, and W. Kang, Rev. Sci. Instrum. **73**, 2999 (2002).
[22] K. Murata, H. Yoshino, H. O. Yadav, Y. Honda, and N. Shirakawa, Rev. Sci. Instrum. **68**, 2490 (1997).
[23] H. Kang, Y. J. Jo, H. C. Kim, H. C. Ri, and W. Kang, Synth. Met. **120**, 1051 (2001).
[24] N. P. Ong and J. W. Brill, Phys. Rev. B **18**, 5265 (1978).
[25] E. S. Choi, H. Y. Kang, Y. J. Jo, J. Yeom, and W. Kang, Synth. Met. **120**, 1069 (2001).
[26] F. Gross, H. Schwenk, K. Andres, F. Wudl, S. D. Cox, and J. Brennan, Mol. Cryst. Liq. Cryst. **119**, 65 (1985).
[27] S. Tomić, D. Jérome, and K. Bechgaard, J. Phys. C **17**, L655 (1984).
[28] C. Hess, C. Schlenker, J. Dumas, M. Greenblatt, and Z. S. Teweldemedhin, Phys. Rev. B **54**, 4581 (1996).
[29] O. H. Chung, I. S. Seo, Y. J. Jo, H. Kang, and W. Kang (unpublished).